Electronic structure and chemical bonding effects upon the bcc to Ω phase transition: *Ab initio* study of Y, Zr, Nb, and Mo

G. B. Grad, P. Blaha, J. Luitz, and K. Schwarz
Technical University of Vienna, Getreidemarkt 9/156, A-1060 Vienna, Austria

A. Fernández Guillermet
Consejo Nacional de Investigaciones Científicas y Técnicas, Centro Atómico Bariloche, 8400 Bariloche RN, Argentina

S. J. Sferco
INTEC (CONICET-UNL), Güemes 3450, (3000) Santa Fe, Argentina
(Received 10 December 1999; revised manuscript received 10 April 2000)

The bcc $\rightarrow\Omega$ phase transition is diffusionless: two-thirds of the atoms in the (111) planes of the bcc phase collapse into double layers, whereas the third remains a single layer. This transformation is observed in the group-IV elements Ti, Zr, and Hf at high pressure, but it may be induced at zero pressure by quenching the samples at room temperature in alloys of these elements with other transition metals (TM's). This paper presents a systematic theoretical study of the bcc$\rightarrow\Omega$ transformation in Y, Zr, Nb, and Mo using the full-potential linearized-augmented-plane-wave method. Equilibrium volumes, total-energy differences, density of electron states, and the band structure of Y, Zr, Nb, and Mo in the stable and metastable bcc and Ω structures are presented. In addition, the bcc$\rightarrow\Omega$ energy difference is studied as a function of the specific lattice distortion as well as of pressure. These results are related to a picture that involves the softening of the $(\frac{2}{3},\frac{2}{3},\frac{2}{3})$ longitudinal phonon mode. Charge-density calculations are performed for both the bcc and Ω phases, and the electronic contributions that stiffen the bcc lattice against the Ω distortion are identified. The physical picture of the electronic and chemical bonding effects emerging from the present work should be useful in understanding the observed trends in the relative stability of the Ω phase in the TM's and their alloys.

I. INTRODUCTION

The theoretical prediction of phase stability trends in the periodic table has been one of the most important goals in materials science. The stability of the most common phases observed in transition metals (TM's) has long been of considerable interest.[1–5] At present, *ab initio* calculations based on density-functional theory (DFT) with the local-density approximation (LDA) or the generalized-gradient aproximation[6] (GGA) are commonly used to study the stable and metastable phases of elements with arbitrarily chosen structures.[5,7–11]

A particularly attractive case for a theoretical investigation occurs when the phases involved are connected by a simple structural transition, which takes place through a diffusion-less mechanism, e.g., the softening of a single phonon mode. This is the case in the transition between bcc and the ($C32$) AlB_2-type structure, the so-called omega (Ω) phase of certain transition metals (TM's). This Ω phase is observed experimentally at high pressure in pure Zr, Ti, and Hf, and by quenching Zr-rich Zr-Nb alloys or in some Ti and Hf alloys.[12–19]

The bcc $\rightarrow\Omega$ transformation is a displacive one: two-thirds of the atoms in the $[111]_{bcc}$ layer collapse into double layers, whereas the third remains a single layer.[20] It has long been suggested that the collapse is caused by the softening of a single phonon, viz., the $(\frac{2}{3},\frac{2}{3},\frac{2}{3})$ longitudinal mode.[21–28] Indeed, the phonon frequencies around $(\frac{2}{3},\frac{2}{3},\frac{2}{3})$ in bcc lattices are soft. Therefore, the weakness towards Ω phase formation can be considered as an intrinsic bcc property, and in particular Zr (and Nb) shows a pronounced dip in the vicinity of this phonon wave vector. The softening of the $L(\frac{2}{3},\frac{2}{3},\frac{2}{3})$ mode may be enhanced or reduced by electronic (Fermi surface) effects acting in the same q-space region.[29–31] Previous calculations related to electronic properties of TMs in bcc or Ω phase can be found in Refs. 29–43.

In the present work, the bcc$\rightarrow\Omega$ structural transformation and the electronic properties of the experimentally metastable Ω phase at room temperature have been studied at 0 K in Y, Zr, Nb, and Mo using *ab initio* electronic structure calculations within the LDA or GGA aproximation to the DFT. A high-temperature bcc phase[44,45] is present in all these elements. The bcc phase of Y and Zr, cooled down at zero pressure, transforms into an hcp phase. In Zr a stable Ω phase is obtained at high pressure.[44,45] Previous calculations by our group[46] and others[32] suggest that in Y the Ω phase is observed if the formation of hcp is avoided. At room temperature and zero pressure, Y and Zr exhibit a hcp phase. Increasing the number of electrons (n_e) (i.e., moving to the right in the periodic table) makes bcc the most stable phase of Nb and Mo at all temperatures and zero pressure.

The general motivation of this study is to explain the decreasing tendency to form Ω in the sequence Y $\rightarrow$ Zr $\rightarrow$ Nb $\rightarrow$ Mo, while the bcc phase is progressively stabilized. The present electronic structure calculations add to the understanding of how the electron band-filling affects the soft-phonon mechanism responsible for the bcc$\rightarrow\Omega$ transforma-

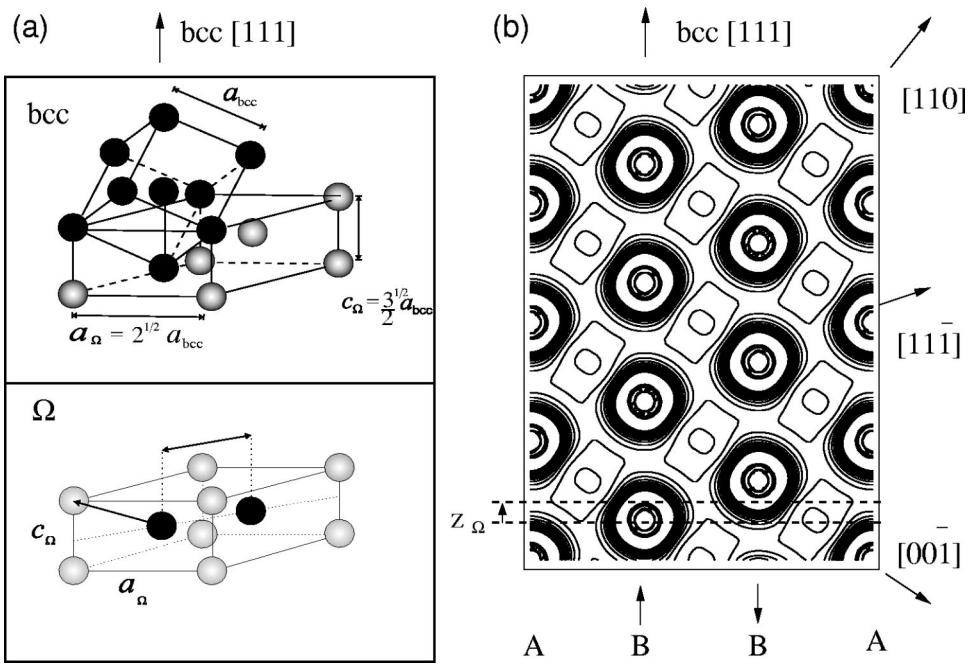

FIG. 1. (a) The relation between bcc and Ω structures. In Ω phase open (filled) circles stand for type A (B) atoms; (b) bcc valence density of Zr in the $(1\bar{1}0)$ plane of the hexagonal cell used in the Ω phase. The displacement z_Ω of the B chains in the bcc→Ω transformation is indicated.

tion. In the following we shall identify the electronic contributions that stiffen the bcc lattice against the shear displacement leading to the bcc→Ω transformation, as described in Fig. 1(a). In addition to the above-mentioned plane-collapse picture of the bcc→Ω transformation, we shall make use of an alternative representation of this transition.

In the bcc→Ω transformation the chains of atoms aligned in the bcc [111] directions move relative to each other as indicated in Fig. 1(b). One chain (A) remains in its position, while the second (third) labeled B, moves up (down), causing a collapse of the (111) planes. Both the Ω and bcc phases can be described by a hexagonal lattice with three atoms per unit cell[19] as shown in Fig. 1(a). The atomic positions are (0,0,0), $(\frac{1}{3},\frac{2}{3},\frac{1}{3}+z_\Omega)$ and $(\frac{2}{3},\frac{1}{3},\frac{2}{3}-z_\Omega)$, where z_Ω is a parameter that permits a continuous description of the bcc→Ω transformation. $z_\Omega=0$ corresponds to bcc, and $z_\Omega=1/6$ corresponds to the ideal Ω phase, with the inner atoms, both at $z=1/2$, collapsed into the same plane (described by the hexagonal $P6/mmm$ space group). For $0<z_\Omega<1/6$ the symmetry is trigonal, described as $P\bar{3}m1$.[19] In the Ω phase there are two nonequivalent sites. The ones at the origin are denoted as A sites and the others inside the cell are labeled as B sites [see Fig. 1(a)]. Using this description we shall calculate the total energy as a function of z_Ω for the various elements and focus on the band-filling effect with respect to the relative stability between Ω and bcc, as well as the instability trends in the 4*d* TM series.

This paper is organized as follows: In Sec. II we describe the theoretical method. Then we present the *ab initio* results concerning the bcc to Ω phase transformation with respect to energetics (Sec. III), charge analysis (Sec. IV), band structure, and their volume dependence (Sec. V). In Sec. VI we summarize the work and give our conclusions.

II. THEORETICAL METHOD

Self-consistent calculations of total energies and the electronic structure based on the scalar relativistic full-potential linearized augmented plane-wave method (FP-LAPW) were carried out using the WIEN97 code.[47,48] This is one of the most accurate schemes to solve the Kohn-Sham equations of DFT in which exchange and correlation effects are treated, for example, by the generalized gradient approximation (GGA), which often leads to better energetics and equilibrium structures than LDA.[6] The electron density is obtained by summing over all occupied Kohn-Sham orbitals and plays the key role in this formalism. Local orbitals are added to the standard LAPW basis in order to describe the 4*s* and 4*p* (semicore) orbitals of Y, Zr, Nb, and Mo. The required precision in total energy was achieved by using a large plane-wave cutoff of $RK_{max}=9$ (resulting in about 500 plane waves) and a *k*-point sampling in the Brillouin zone (BZ) of about 3000 points. This corresponds to 170 *k* points in the irreducible wedge of the Ω phase and to 104 in the bcc phase. The total and partial density of states[49] (DOS) was obtained using a modified tetrahedron method of Blöchl *et al.*[50] The atomic sphere radii (in a.u.) used were 2.5 for Y, 2.3 for Zr, 2.2 for Nb, and 2.0 for Mo. For each of the elements the full analysis was carried out at the theoretical equilibrium volume based on the LDA, but the results are practically unchanged when the GGA equilibrium volume would be used. The theoretical equilibrium volumes obtained by our calculations (see Table I) are slightly smaller than the experimental ones as commonly observed in LDA calculations.[7–11]

TABLE I. Ratios of V/V_0, where V is the theoretical equilibrium volume (within LDA) and $V_0=68.96$ Å^3 is the volume of the Ω phase in pure Zr as extrapolated from experiments. This V_0 was used as reference for Ω (3 atoms per unit cell) and $\frac{2}{3}V_0$ was used as reference for bcc (2 atoms per unit cell).

	Y	Zr	Nb	Mo
bcc	1.28	0.92	0.75	0.65
Ω	1.28	0.94	0.76	0.66

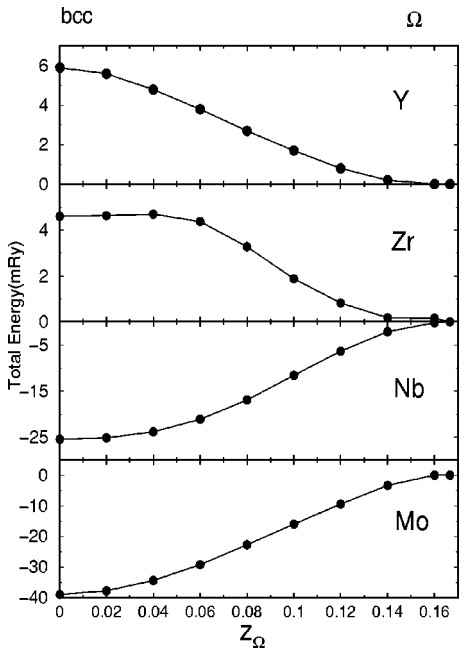

FIG. 2. Energy difference (mRy) for the bcc→Ω transformation in Y, Zr, Nb, and Mo as a function of the internal z_Ω parameter (within LDA). The energy is with respect to the Ω phase.

III. ENERGETICS AND STABILITY OF THE bcc AND Ω PHASES

When going from bcc to Ω along the path described above, we have studied the total energy of Y, Zr, Nb, and Mo using the common trigonal structure as a function of z_Ω (Fig. 2). The calculations for each element were performed at the zero-pressure equilibrium volume (within LDA) of the respective Ω phase. Under those conditions only Zr shows a double-minimum configuration, i.e., is (meta-) stable for both the bcc and Ω phase. However, the bcc phase is not only less stable than Ω, but requires only a very small activation energy to transform into the Ω phase. The energy difference between the two phases is $E(\text{bcc})-E(\Omega)=4.5$ mRy in Zr. In Y this energy difference is even more pronounced, i.e., bcc Y is unstable with respect to the trigonal distortion, and the energy difference $E(\text{bcc})-E(\Omega)=6$ mRy is larger. Lacking experimental information on the phonon spectrum of bcc Y, our prediction of an instability in bcc Y cannot be tested here. On the other hand, in Nb and Mo the relative phase stability is reversed and Fig. 2 shows that Ω is evidently unstable against the Ω→ bcc distortion. The bcc phases of Nb and Mo are energetically favored over the Ω phases by -26 and -39 mRy, respectively.

In order to investigate the volume effect on this transition we performed similar calculations for Zr using different volumes (Fig. 3). It is evident that lattice expansion would favor the Ω phase, while increasing compression progressively stabilizes the bcc phase. This is consistent with the experimental phase diagram of pure Zr in which bcc is the high-pressure phase.[45]

We estimated the theoretical pressure at which the bcc becomes more stable than Ω and obtained 178 kbar from LDA calculations and 291 kbar using GGA calculations. The latter agrees rather well with the experimental result of 300 kbar reported for Zr by Vohra and Ruoff,[51] and Xia *et al.*[52,53] Our results for Zr are also in good agreement with the results of Jomard *et al.*[43] obtained with full potential linear muffin-tin orbital calculations using LDA (112 kbar) and GGA (354 kbar). The stabilization of the more open structure (Ω) in GGA versus LDA calculations can be understood on the basis of the analysis of Zupan *et al.*,[54] who showed that GGA favors charge inhomogeneity.

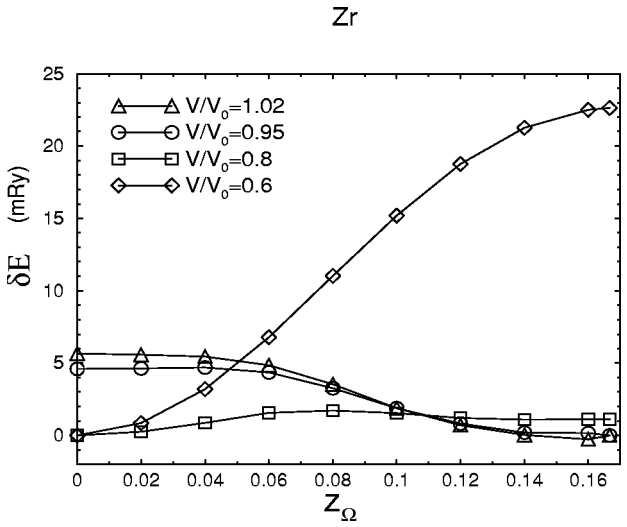

FIG. 3. Energy difference (mRy) of Zr (as in Fig. 2) shown for different volumes (within LDA). Zero of energy is at the respective minimum.

From the harmonic part of the energy versus the z_Ω curve we evaluate phonon frequencies of 3.10 THz for Nb and 4.74 THz for Mo using the GGA aproximation. The calculations of the energy as a function of z_Ω were performed using the theoretical lattice constants (within GGA) for the bcc structures, i.e., 2.85 Å for Nb and 2.72 Å for Mo. These values compare reasonably well with the experimental[34] frequencies (3.57 THz in Nb and 6.31 THz in Mo). It should be noted that those frequencies do not change much whether GGA or LDA is used in contrast to the transition pressure mentioned above.

IV. DENSITY OF STATES AND CHARGE ANALYSIS IN THE bcc AND Ω PHASES

A. Background

The experimentally observed low phonon frequency in bcc Zr was associated by Heiming *et al.*[55] to the weak restoring forces between the chains, shown in Fig. 1. In order to account for the bcc stability for elements to the right of Zr, they proposed strong *d*-*d* bonds between the [111] chains, which oppose shearing motions between neighboring chains. In the following, we shall identify the key contributions to the lattice stiffening against the bcc→Ω distortion using analysis based on partial DOS, partial charges, and charge-density distributions. With the splitting of the total *d* DOS into its irreducible representations (Fig. 4) and the corresponding partial charges (Table II) we can now explicitly confirm the picture speculated by Heiming *et al.*[55]

B. Charge distribution in the bcc phase

In the bcc structure the *d* orbitals split into two irreducible representations, namely, d-e_g and d-t_{2g}, where the latter

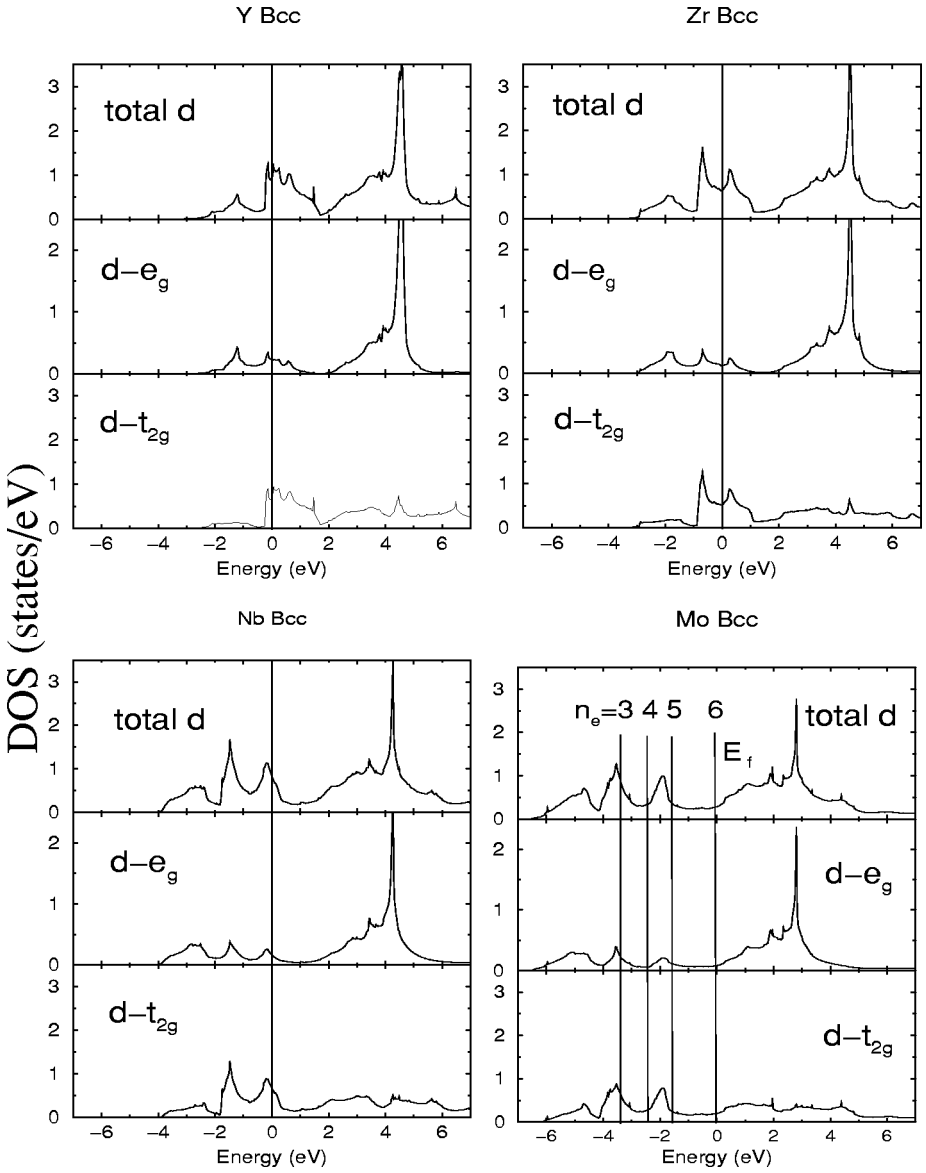

FIG. 4. Partial *d* DOS (density of states) per atom of Y, Zr, Nb, and Mo in the bcc phase. The energy (eV) is with respect to E_F. For Mo the lowering of E_F is shown according to the rigid band model by reducing the number of valence electrons n_e from 6 to 3 (i.e., corresponding to Mo, Nb, Zr, and Y).

point along the nearest-neighbor [111] direction while the former point towards the next-nearest neighbors along [100]. We plot the partial *d* DOS together with their symmetry splitting in Fig. 4. It is evident that the e_g character does not change much in the series from Y to Mo. It shows a sharp peak at higher energies, which is, however, unoccupied in all cases. At the low-energy side the d-e_g DOS is always larger than the d-t_{2g} DOS. The latter does not show such a good rigid band behavior and in particular the Y d-t_{2g} DOS is different from the other cases. At low energies the Y d-t_{2g} contribution starts out very flat and also the main feature has little structure. In Zr a small valley appears in the main d-t_{2g} structure while for Nb and Mo the valley between the two main peaks is enlarged corresponding to the typical DOS of a bcc structure.

TABLE II. Partial valence charges in units of *e*, in bcc Y, Zr, Nb, and Mo.

	Y	Zr	Nb	Mo
s	0.170	0.159	0.165	0.132
p	0.111	0.126	0.158	0.168
$de_g/2$	0.188	0.272	0.362	0.420
$dt_{2g}/3$	0.124	0.303	0.486	0.615
total	1.029	1.738	2.505	2.985

The partial charges, which are the integrated partial DOS inside the atomic sphere, depend of course on the sphere size. These values are different for the different atoms and therefore the partial charges can only be used to establish trends and verify some relations but should not be over interpreted.

Table II lists the valence partial charges $5s$, $5p$, and $4d$, where the latter are split according to symmetry. We find that the $5s$ partial charge decreases within the series, whereas the $5p$ charge increases. More interesting is the behavior of the partial *d* contributions. In Y the d-e_g charge dominates over the d-t_{2g} contribution, indicating that there is little direct d-d bonding along the nearest-neighbor [111] direction. This is the reason why Y is not stable in the bcc structure. In Zr the

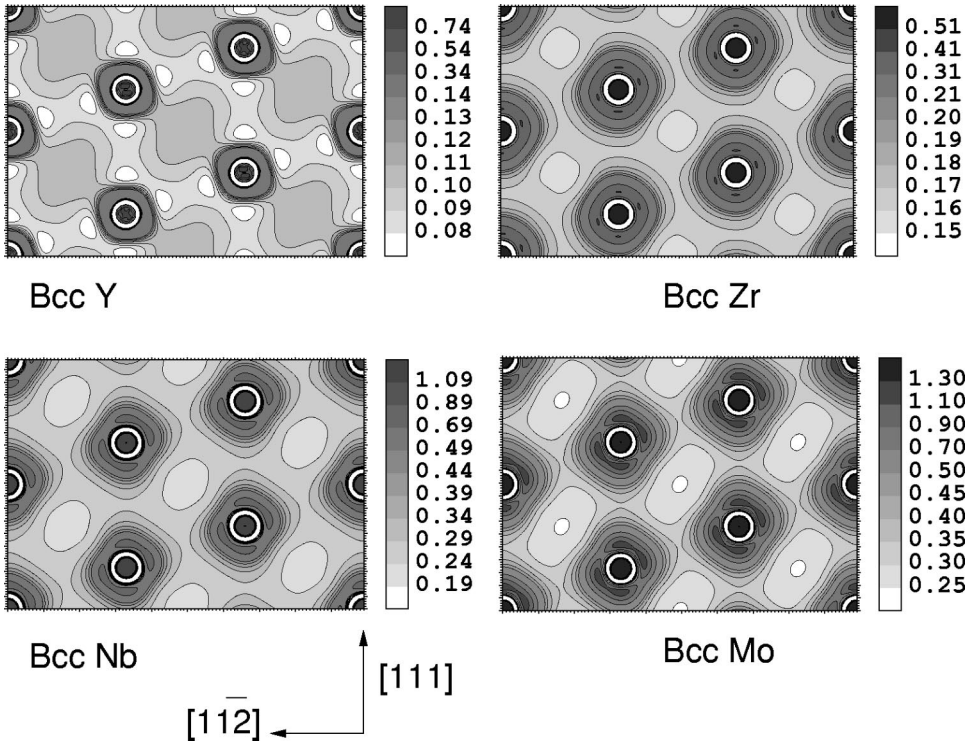

FIG. 5. Valence-charge distribution of bcc Y, Zr, Nb, and Mo in the $(1\bar{1}0)$ plane. The units are in $e/\text{Å}^3$, illustrated by corresponding gray shadings.

situation is changed since the d-t_{2g} representation is slightly more occupied than d-e_g. Of course this trend is even more pronounced in Nb and Mo and is responsible for both the strong directional bonds along the [111] chains and the stability of the bcc structure. Qualitatively this picture emerges already from a rigid-band model using any of the four bcc DOS as illustrated for bcc Mo in Fig. 4.

In order to visualize the chemical bonding directly we present the valence-charge densities (i.e., the $4d$, $5s$, and $5p$ states) for bcc Y, Zr, Nb and Mo in the $(1\bar{1}0)$ plane in Fig. 5. This plane includes both the nearest-neighbor direction [111] as well as the next-nearest-neighbor direction [001] as indicated in Fig. 1(b). The valence charge density in Y is concentrated in the interstitial region along the [001] direction between next-nearest neighbors. In the [111] direction the density is fairly low. This weak bonding between nearest neighbors explains the instability of bcc Y. An opposite effect is observed in Zr, Nb, and Mo, where the density gradually increases in the nearest-neighbor bonding direction due to the occupation of additional d states, mainly of t_{2g} character.

We conclude this section by stating that the increase in stability of the bcc phase for the heavier elements is related to the remarkable increase of the d-t_{2g} contribution to the bonding in the sequence Y $\rightarrow$Zr$\rightarrow$Nb$\rightarrow$Mo. This behavior has been demonstrated using symmetry-decomposed DOS as well as charge-density distributions.

C. Charge distribution in the Ω phase

In contrast to the cubic (bcc) case, the Ω phase has hexagonal symmetry and thus the d states decompose into three irreducible representations, namely d_{z^2}, $d_{x^2-y^2}+d_{xy}$, and $d_{xz}+d_{yz}$. We note that the d_{z^2} orbital corresponds to one of the three degenerate t_{2g} states of cubic symmetry. The partial d DOS as well as their decompositions are shown in Figs. 6 and 7 for the A and B sites, respectively, and differ for the two sites. For the A site a high peak of $d_{x^2-y^2}+d_{xy}$ character near E_F shows up, which is unoccupied in Y (at 0.9–2.2 eV) and Zr (at 0–1.4 eV), but starts to be filled in Nb and Mo. At the B site more weight is shifted to lower energies. The main peak is narrower and starts to become occupied only in Mo. The $d_{xz}+d_{yz}$ DOS has much more structure at the A than at the B site and a low-energy peak is already occupied in Y and Zr. The d_{z^2} DOS is surprisingly structureless. However, it is evident that more and more d_{z^2} states become occupied in Nb and Mo. This suggests that in addition to the contributions in the plane, those in the z direction (corresponding to [111] directions in the bcc lattice) are partially responsible for the bcc stabilization in Nb and Mo.

The various contributions at the two nonequivalent sites of Zr are presented in Table III. Our results show that for Y and Zr the main contribution to A sites comes from $d_{xz}+d_{yz}$, while at the B sites the main contribution is $d_{x^2-y^2}+d_{xy}$. Furthermore, we note that in Zr the $d_{x^2-y^2}+d_{xy}$ character at the B site is larger than the $d_{xz}+d_{yz}$ character for the A sites. In Y the relationship between these characters is exactly the opposite. The behavior of Nb and Mo is quite different from the previous cases, viz., both sites show the d_{z^2} character as their main contribution, corresponding to the [111] direction of the bcc cell.

The partial charges summarized in Table III may be compared to those in Table IV, where the bcc structure is also represented in the hexagonal coordinate system, i.e., with the z axis along the cubic [111] direction. In most cases, the bcc partial charges are between the corresponding A- and B-site charges of the Ω phase.

In Y the $d_{xz}+d_{yz}$ charge is larger for the A site, while the $d_{x^2-y^2}+d_{xy}$ contribution is larger for the B site. In comparison to the bcc case, a redistribution of the bcc $d_{x^2-y^2}+d_{xy}$ charge to the B site and of the bcc $d_{xz}+d_{yz}$ towards the A

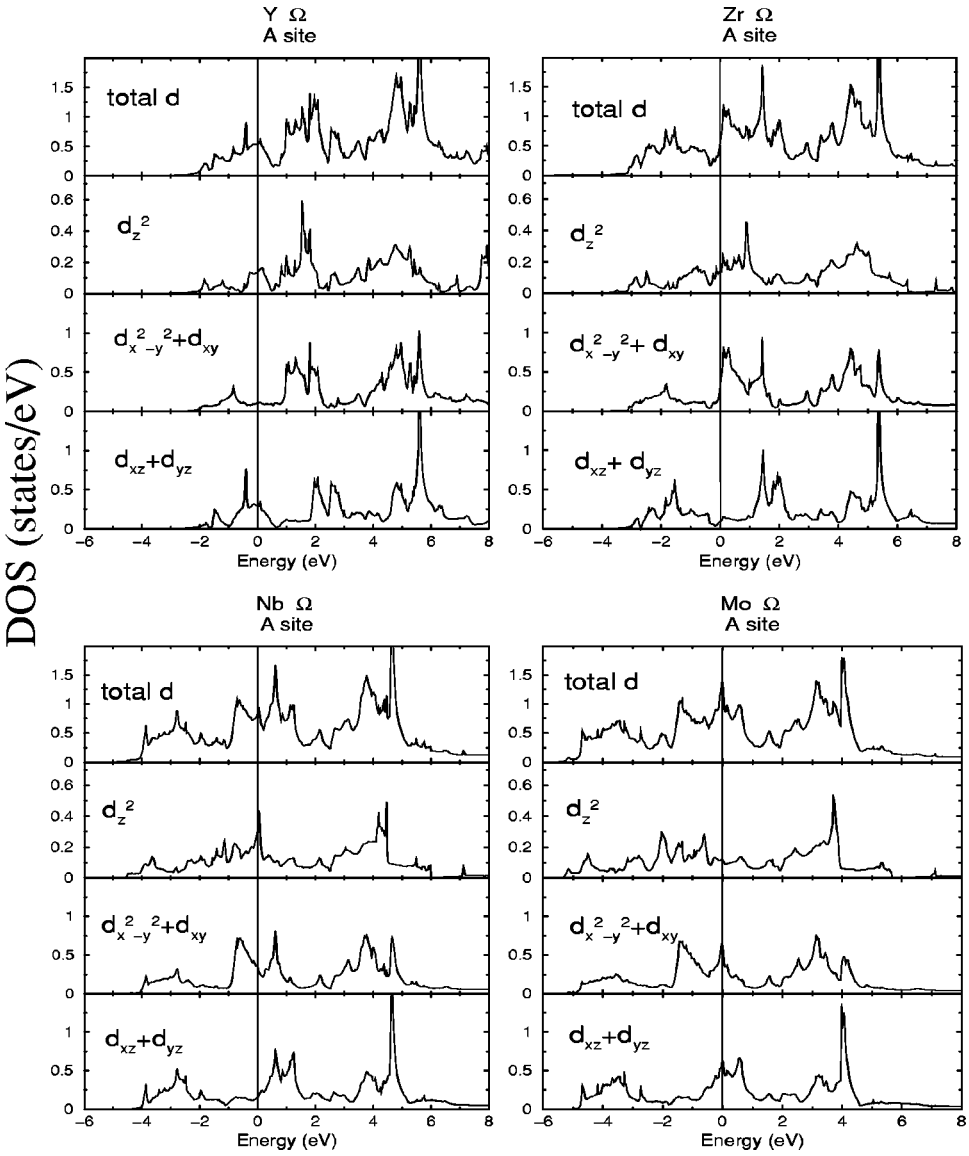

FIG. 6. Symmetry-decomposed partial *d* DOS (density of states) per atom of the A site in Y, Zr, Nb, and Mo in the Ω phase.

site can be seen. In Zr d_{z^2} orbitals start to contribute significantly to the bonding (both, for A and B sites), a situation also present in the bcc structure. For Nb and Mo the $d_{xz}+d_{yz}$ charge is now smaller than the other contributions; this indicates low interaction between A and B sites, but strong bonds between A and A sites (along z) and B and B sites (within the hexagonal plane but also along *z*). In the bcc phase this latter effect is only visible for Mo, but not for Nb. We also see in Table III that in the sequence Y→Zr→Nb →Mo the A and B sites gradually loose the features that make them nonequivalent.

In Fig. 8 we plot the valence charge density of the Ω phase for the four elements in the $(1\bar{2}10)$ plane that contains both the A and B sites. This plane in the Ω phase corresponds to the $(1\bar{1}0)$ plane in bcc.

In Y charge accumulates in the center of the triangle formed between two A and one B site as well as in the middle between the four B sites. This implies strong interactions between A and B sites, but little interactions between A and A sites and B and B sites along the *c* direction. In Zr the A-B bonding is even stronger, but a significant charge can now also be found between the A and A sites and the B and B sites, while the lowest density is found in the center of a triangle formed by one A and two B sites. The situation is completely different for Nb and Mo, where the charge density is concentrated between A and A sites (along *z*) and B and B sites (both in the hexagonal plane and along *z*) atoms, while between A and B sites there is little interaction.

We conclude this section by stating that the increase in stability of the Ω phase for the lighter elements is related to the relative increase of A-B interactions compared to the decrease of A-A and B-B interactions. In particular, strong B-B bondings (especially in the basal hexagonal plane) do not favor the stability of the Ω phase. This result is opposite to some theoretical speculations[12,41] that assign the basal B-B interactions in Ω Zr as being responsible for the stability of this phase.

V. ENERGY BAND STRUCTURES

A. At equilibrium volume

The band structure calculated along various directions in the basal plane of the hexagonal cell at $k_z=0$ (Γ-*M*-*K*-Γ)

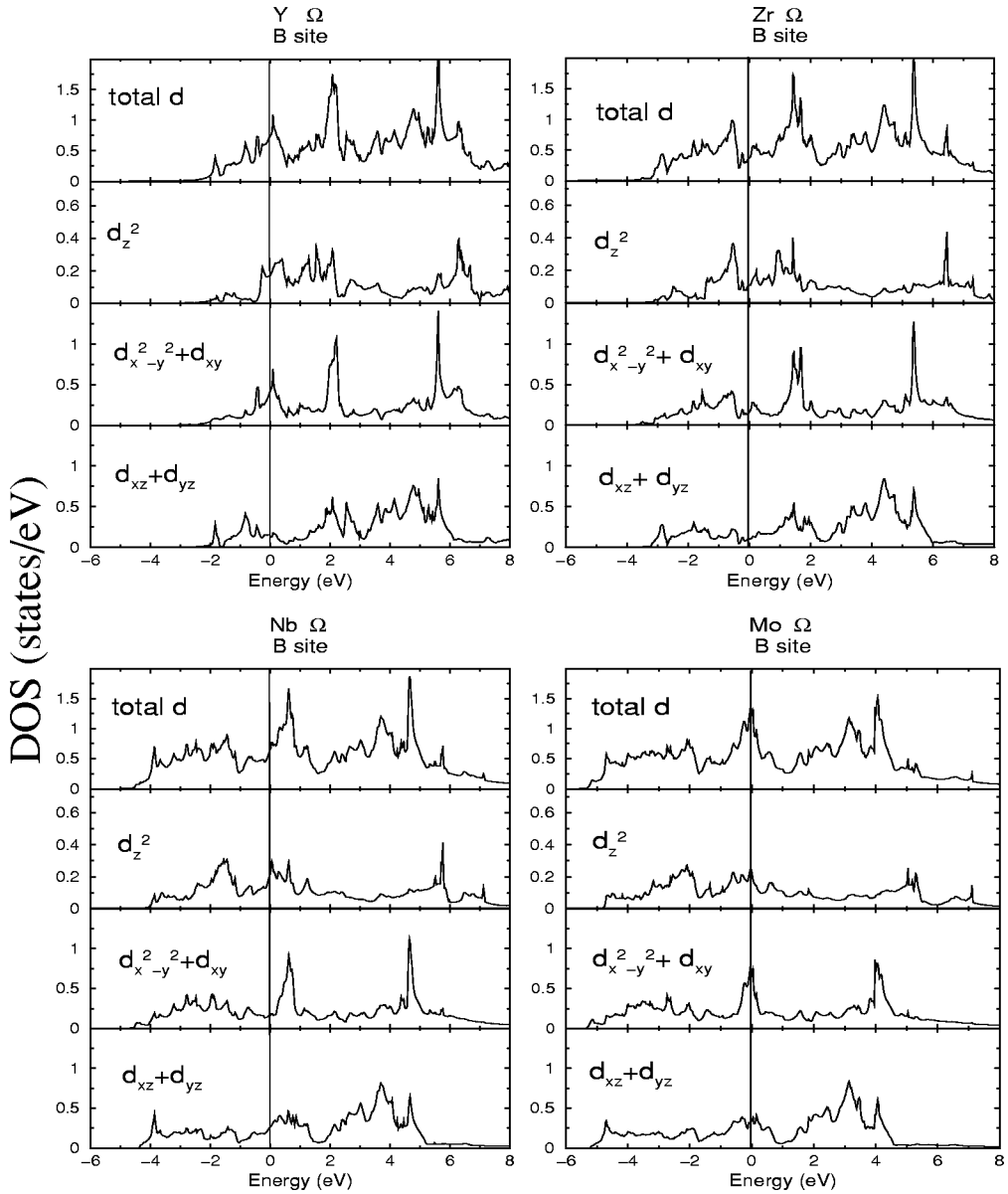

FIG. 7. Symmetry-decomposed partial *d* DOS (density of states) per atom of the B site in Y, Zr, Nb, and Mo in the Ω phase.

and $k_z=1/2$ (A-R-L-H-Q-A-C) is plotted in Fig. 9. For the elements Y and Zr we present the bands of the hexagonal Ω phase, while for Nb and Mo we present those for the bcc phase (but described in the $P3m1$ cell with $z_\Omega=0$). It is evident that in the Ω phase the band structure exhibits a characteristic gap between the low-energy bonding states and the antibonding states at higher energy that is only present in the $k_z=1/2$ plane, but not at $k_z=0$. According to Figs. 6 and 7 the electronic states in the Ω phase of Zr are filled to the deep valley in the DOS and the corresponding band structure

TABLE III. Partial valence charges in units of *e*, inside the atomic spheres for sites A and B in the Ω phase of Y, Zr, Nb, and Mo.

	Y		Zr		Nb		Mo	
	A	B	A	B	A	B	A	B
s	0.164	0.173	0.156	0.161	0.158	0.173	0.125	0.136
p	0.116	0.106	0.158	0.129	0.165	0.146	0.149	0.145
d_{z^2}	0.117	0.117	0.273	0.317	0.479	0.513	0.585	0.630
$(d_{x^2-y^2}+d_{xy})/2$	0.120	0.171	0.236	0.321	0.449	0.469	0.571	0.586
$(d_{xz}+d_{yz})/2$	0.180	0.164	0.291	0.249	0.369	0.380	0.496	0.492
total	0.997	1.066	1.641	1.747	2.438	2.530	2.993	3.067

TABLE IV. Partial valence charges in units of *e*, inside the atomic spheres for the bcc phase of Y, Zr, Nb, and Mo, expressed in the trigonal symmetry.

	Y	Zr	Nb	Mo
s	0.170	0.159	0.165	0.132
p	0.111	0.127	0.158	0.167
d_{z^2}	0.124	0.302	0.487	0.615
$(d_{x^2-y^2}+d_{xy})/2$	0.146	0.292	0.444	0.550
$(d_{xz}+d_{yz})/2$	0.167	0.283	0.403	0.486
total	1.031	1.738	2.504	2.986

in Fig. 9 shows that the Fermi energy falls in fact into the gap present in the $k_z=1/2$ plane. With different band filling, however, this cannot be achieved in Y (where E_F is near the bottom of the gap) nor in Ω Nb or Mo. In contrast, the bcc structure for the two latter elements leads to a low density of states at E_F. In the case of Mo the Fermi energy is placed in a pseudogap of the bcc DOS, where in the corresponding band structure only very steep bands cross E_F.

Further analysis of the character of the individual bands in Ω Zr shows that in the $k_z=0$ region both atomic sites (A and B) seem to have similar contributions to a particular band. This is illustrated in Fig. 10, where the $d_{xz}+d_{yz}$ character for both sites is marked with circles proportional to the amount of $d_{xz}+d_{yz}$ charge. For $k_z=0$ the contribution from both sites is comparable. At $k_z=1/2$, however, the character of certain bands differ drastically for sites A and B.

Furthermore, it is evident that in the first region ($k_z=0$) there is no $d_{xz}+d_{yz}$ character at all in the occupied states, but all states with this character are shifted above E_F. For $k_z=1/2$, however, several occupied bands have this character. The downward shift in energy comes from a strong covalent interaction between A (B) $d_{xz}+d_{yz}$ states with B (A) $d_{x^2-y^2}+d_{xy}$ states (the latter are not shown explicitly here). This interaction seems to be rather important for the bonding between the atoms A and B and thus for the stabilization of the Ω phase.

These band-structure results are consistent with the partial charges listed in Table III, where for Y and Zr the A and B contributions to the $d_{x^2-y^2}+d_{xy}$ and the $d_{xz}+d_{yz}$ characters are similar. The A contribution to the $d_{xz}+d_{yz}$ character is bigger than the B contribution to the $d_{x^2-y^2}+d_{xy}$ character for Y, but the opposite is true for Zr, and this tendency is enhanced for Nb and Mo, corresponding to a smaller A-B interaction.

B. Volume effects on the Ω band-structure calculation

To complement the calculations already presented, we analyze the band structure also for compressed Zr [Fig. 10(b)] with $V/V_0=0.7$, where V_0 is the experimental volume of the Ω phase cell and compare it with uncompressed Zr. We find that the gap that is present in the Ω phase for the *k* points at $k_z=1/2$ becomes smaller when the volume decreases and vanishes completely at a certain pressure [see Fig. 10(b)]. The number of states near the Fermi energy increases and this makes the compressed Ω phase similar to the bcc phase, which does not show this gap. This is also consistent with the fact that both experimentally and theoretically the bcc phase becomes the most stable phase of Zr at higher pressure.

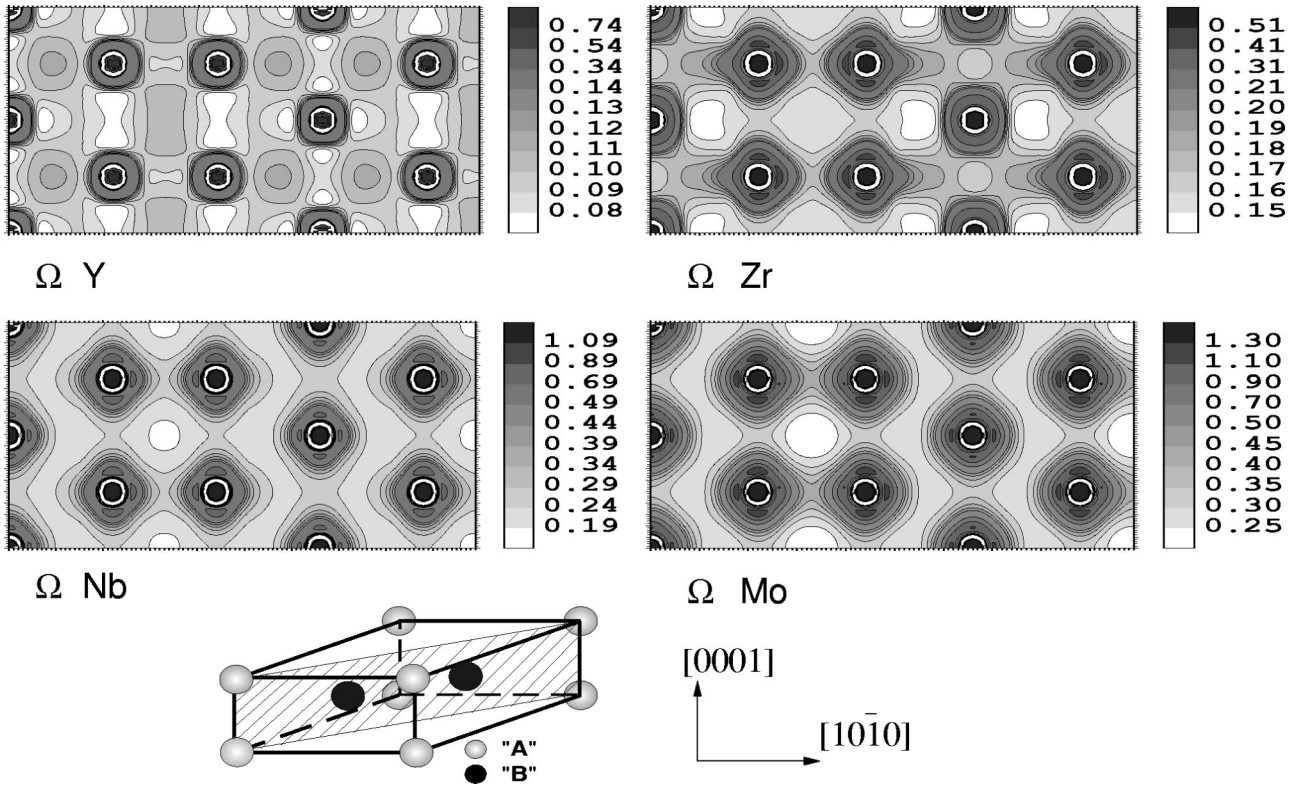

FIG. 8. Valence-charge distribution in Y, Zr, Nb, and Mo $(1\bar{2}10)$ in the Ω phase. The units are in $e/\text{Å}^3$, illustrated by corresponding gray shadings.

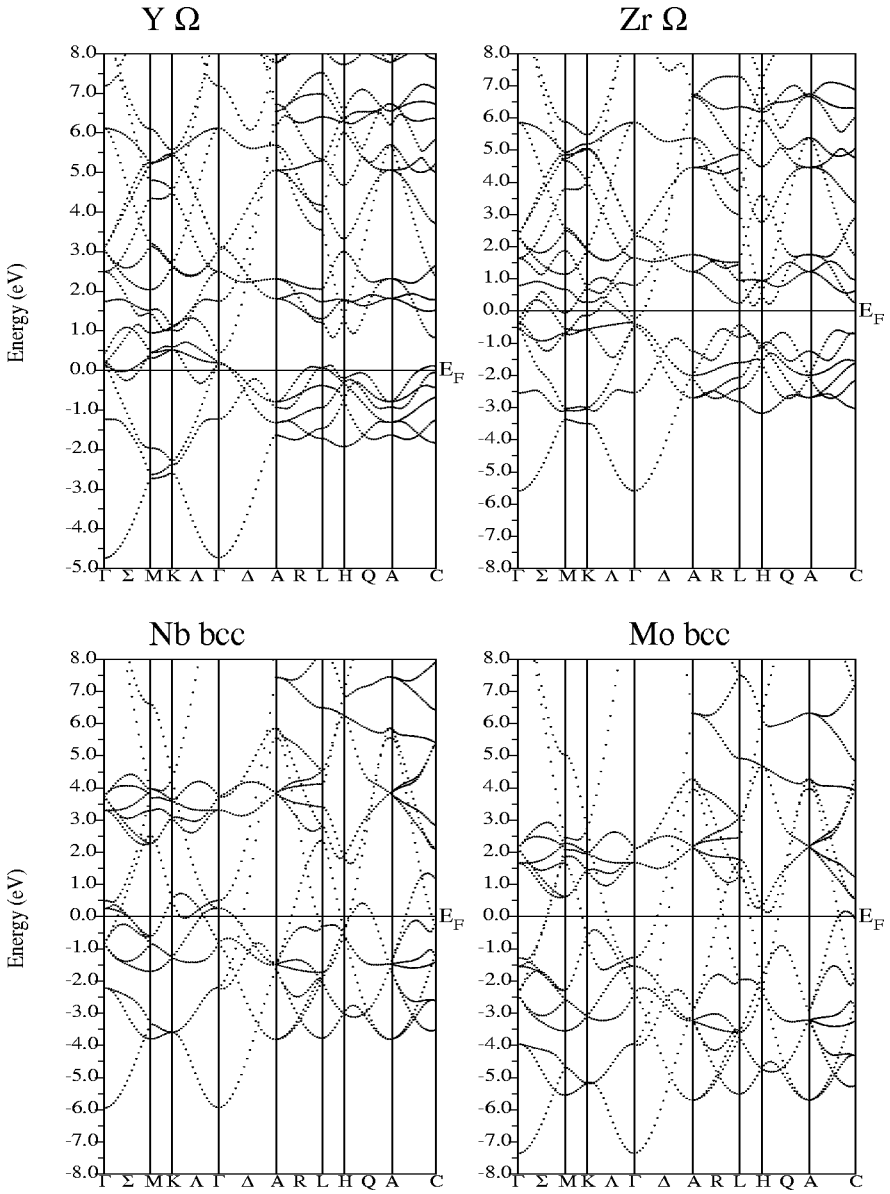

FIG. 9. The band structure (in eV) of Y, Zr (in the Ω phase), and Nb, Mo (in the bcc phase) both in the hexagonal reciprocal unit cell.

From Fig. 10(b) it is also evident that closing of the gap occurs first for states with mainly $d_{xz}+d_{yz}$ character at site B, while states with this character at site A are not much affected. This is in contrast to states with $d_{x^2-y^2}+d_{xy}$ character, since pressure affects both lattice sites (not shown explicitly).

In transition metals compression often induces a $sp \rightarrow d$ transfer of valence electrons. This arises from the fact that the spatially extended *s* and *p* states feel the effects of high pressure more strongly than the localized *d* states. Thus the corresponding *s* and *p* energy bands rise faster in energy than the *d* bands and the transfer of electrons from *s*- and *p*-like to *d*-like states is favored. If such a $sp \rightarrow d$ electron transfer exists with compression, then applying pressure is equivalent to increasing n_e, i.e., moving to the right in the periodic table.[33] The changes in the band structure of Zr under compression are consistent with this general rule.

VI. SUMMARY AND REMARKS

The picture of the electronic effects on the bcc→Ω transformation that emerges from the present work may be summarized as follows. The tendency towards the bcc→Ω transformation originates from the existence of a low-frequency $\frac{2}{3}(1,1,1)$ phonon mode, which implies weak restoring forces for the relative movement of [111] atomic chains. In the sequence Y→Zr→Nb→Mo the resistance against the Ω distortion increases by the development of strong *d* bonds, predominantly with t_{2g} character, which contributes to the bonding in the [111] directions. In Y the e_g character is still dominant (and thus the bcc→Ω transformation is most favorable). This tendency in the bcc phase is accompanied by significant differences in the charge-density distribution. The valence electron density is concentrated in the interstitial region in Y (between next-nearest neighbors) but directly between the nearest neighbors in Nb and Mo.

We have also shown that band-filling considerations can be complemented with calculations under compression. We analyzed partial charges and trends in the different contributions to the *d*-*d* bonding. We also calculated the equilibrium pressure between bcc and Ω phases and obtained good agreement with experiments.

In particular, total-energy calculations show that in Y and

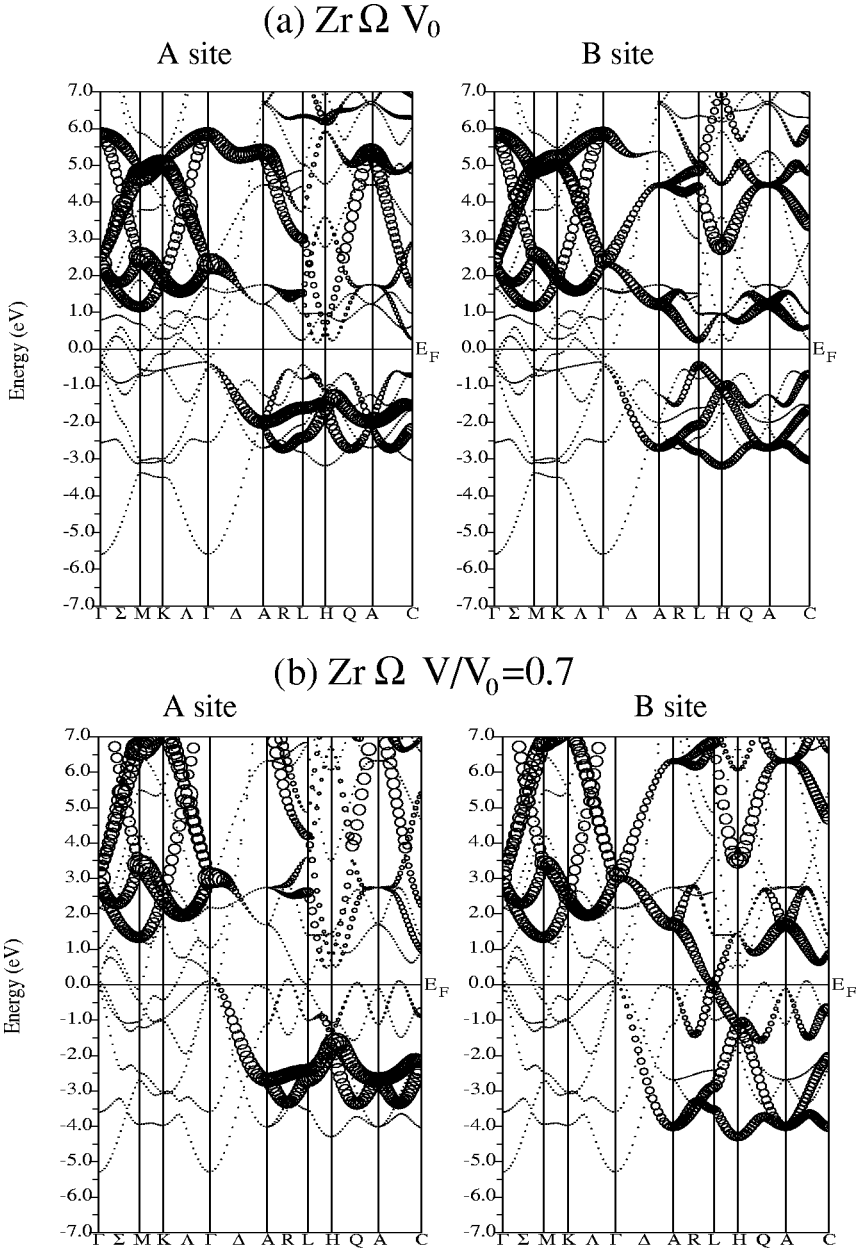

FIG. 10. Character of the energy bands (in eV) of Ω Zr: (a) at equilibrium; (b) under pressure ($V/V_0=0.7$). The radius of the circles is proportional to the respective partial $d_{xz}+d_{yz}$ charge at site A (left) or site B (right).

Zr the bcc phase tends to become more stable on compression, which correlates with the appearance of a valley in the DOS of the t_{2g} complex, under these conditions. The results are in agreement with the ideas of Moriarty,[33] who implies that, on compression, the TM's tend to crystallize in the phase shown by the element placed to the right in the periodic table. The Ω→bcc phase transition occurring in Zr and the other group-IV elements Ti and Hf is consistent with such a generalization and the present results, which confirm the compression effects on the DOS of the bcc phase.

Our work indicates that the stabilization of the Ω phase at the beginning of the $4d$ series is related to the electron filling, so that only states below the gap in the $k_z=1/2$ plane of the Brillouin zone are occupied. As soon as higher states become occupied, the Ω phase becomes destabilized and this could be verified by simple virtual crystal calculations. The bonding behavior of $d_{xz}+d_{yz}$ orbitals at B sites and $d_{x^2-y^2}+d_{xy}$ character at A sites within the same band seems to be responsible for the lowering of those eigenvalues resulting in this pronounced band gap for Y and Zr in this phase.

This effect is indeed lost in Nb and Mo, where the valence-charge density is concentrated in d bonds in the [111] directions. With additional filling of higher levels the antibonding contributions raise the energy leading to a destabilization of the Ω phase. Besides, in the bcc phase, the charge distribution stiffens the lattice against the shearing motion between neighboring [111] chains, i.e., the specific distortion from bcc leading to the formation of the Ω phase.

ACKNOWLEDGMENTS

Two of us (G.B.G. and S.J.S.) would like to thank the Abdus Salam ICTP, Trieste, Italy, for the support which allow them to participate in the workshop on ''All-Electron LAPW Electronic Structure Calculations, 1998.'' The present research was supported by Cooperativa de Electricidad Bariloche (Argentina), by Fundación Balseiro (Argen-

tina), by Agencia Nacional de Promoción Científica y Tecnológica (Argentina), under Grant No. 03-00000-00688, and by CONICET Grant No. PIP 4800/96. S.J.S. is partially supported by CONICET. G.B.G. is supported by CONICET. We want to thank Max Petersen and Griselda García for their help with the graphics. We also thank Albrech Preusser for his program XFARBE (Fill Area with Bicubics, Visualization of 2D-Arrays).

[1] R. A. Deegan, J. Phys. C **1**, 763 (1968).
[2] N.W. Dalton and R.A. Deegan, J. Phys. C **2**, 2369 (1969).
[3] J. Friedel, in *The Physics of Metals. I. Electrons*, edited by J.M. Ziman (Cambridge University Press, Cambridge, UK, 1969), p. 340.
[4] D.G. Pettifor, J. Phys. C **3**, 367 (1970).
[5] F. Ducastelle and F. Cyrot-Lackman, J. Phys. Chem. Solids **32**, 285 (1971).
[6] J.P. Perdew, S. Burke, and M. Ernzerhof, Phys. Rev. Lett. **77**, 3865 (1996).
[7] V.L. Moruzzi, J.F. Janak, and A.R. Williams, *Calculated Electronic Properties of Metals* (Pergamon, New York, 1978).
[8] H.L. Skriver, Phys. Rev. B **31**, 1909 (1985).
[9] A.T. Paxton, M. Methfessel, and H.M. Polatoglou, Phys. Rev. B **41**, 8127 (1990).
[10] R.E. Watson, G.W. Fernando, M. Weinert, and J.W. Davenport, J. Phase Equilib. **13**, 244 (1992).
[11] V. Ozolins and M. Körling, Phys. Rev. B **48**, 18 304 (1993).
[12] J.C. Jamieson, Science **140**, 72 (1963).
[13] A. Jayaraman, W. Klement, and G.C. Kennedy, Phys. Rev. **134**, 664 (1963).
[14] B.S. Hickman, J. Mater. Sci. **4**, 554 (1969).
[15] S. L. Sass, J. Less-Common Met. **28**, 157 (1972).
[16] K.M. Ho, S.G. Louie, J.R. Chelikowsky, and M.L. Cohen, Phys. Rev. B **15**, 1755 (1977).
[17] C. Stassis, J. Zarestky, and N. Wakabayashi, Phys. Rev. Lett. **41**, 1726 (1978).
[18] G.B. Grad, J.J. Pieres, A. Fernández Guillermet, G.J. Cuello, and J.R. Granada, Z. Metallkd. **86**, 395 (1995).
[19] G.B. Grad, A. Fernández Guillermet, J.J. Pieres, and J.R. Granada, Z. Metallkd. **87**, 726 (1996).
[20] S.K. Sikka, Y.K. Vohra, and R. Chidambaram, Prog. Mater. Sci. **27**, 245 (1982).
[21] D. de Fontaine, Acta Metall. **18**, 275 (1970).
[22] D. de Fontaine, N.E. Patton, and J.C. Williams, Acta Metall. **19**, 1153 (1971).
[23] D. de Fontaine and O. Buck, Philos. Mag. **27**, 967 (1973).
[24] J.C. Williams, D. de Fontaine, and N.E. Patton, Metall. Trans. A **4**, 2701 (1973).
[25] S.C. Moss, D.T. Keating, and J.D. Axe, Solid State Commun. **13**, 1465 (1973).
[26] D. de Fontaine and R. Kikuchi, Acta Metall. **22**, 1139 (1974).
[27] D. de Fontaine, Metall. Trans. A **19**, 169 (1988).
[28] C. Falter, W. Ludwig, M. Selmke, and W. Zierau, Phys. Lett. **90A**, 250 (1982).
[29] K.M. Ho, C. L. Fu, and B.N. Harmon, Phys. Rev. Lett. **49**, 673 (1982).
[30] K.M. Ho, C.L. Fu, and B.N. Harmon, Phys. Rev. B **28**, 6687 (1983).
[31] J. Zarestky, C. Stassis, B.N. Harmon, K.M. Ho, and C.L. Fu, Phys. Rev. B **28**, 697 (1983).
[32] J. Melsen, J.M. Wills, B. Johansson, and O. Eriksson, Phys. Rev. B **48**, 15 574 (1993).
[33] J.A. Moriarty, Phys. Rev. B **45**, 2004 (1992).
[34] K.M. Ho, C.L. Fu, and B.N. Harmon, Phys. Rev. B **29**, 1575 (1984).
[35] K.M. Ho and B.N. Harmon, Mater. Sci. Eng., A **127**, 155 (1990).
[36] Y.K. Vohra, S.K. Sikka, and R. Chidambaram, J. Phys. F: Met. Phys. **9**, 1771 (1979).
[37] J.S. Gyanchandani, S.C. Gupa, S.K. Sikka, and R. Chidambaram, J. Phys.: Condens. Matter **2**, 301 (1990).
[38] J.S. Gyanchandani, S.C. Gupa, S.K. Sikka, and R. Chidambaram, J. Phys.: Condens. Matter **2**, 6457 (1990).
[39] H. Ezaki, M. Morinaga, M. Kato, and N. Yukawa, Acta Metall. Mater. **39**, 1775 (1991).
[40] D. Nguyen-Manh, D.G. Pettifor, G. Shao, A.P. Miodownik, and A. Pasturel, Philos. Mag. B **74**, 1385 (1996).
[41] R. Ahuja, J.M. Wills, B. Johansson, and O. Eriksson, Phys. Rev. B **48**, 16 269 (1993).
[42] I. Bakonyi, H. Ebert, and A.I. Liechtenstein, Phys. Rev. B **48**, 7841 (1993).
[43] G. Jomard, L. Magaud, and A. Pasturel, Philos. Mag. B **77**, 67 (1998).
[44] J. Donohue, *The Structures of the Elements* (Krieger, Malabar, FL, 1982).
[45] D. A. Young, *The Phase Diagrams of the Elements* (University of California Press, Berkeley, CA, 1991).
[46] J. Garces, G.B. Grad, A. Fernández Guillermet, and S. Sferco, J. Alloys Compd. **287**, 6 (1999).
[47] P. Blaha, K. Schwarz, and J. Luitz, *Computer Code WIEN97* (Vienna University of Technology, Vienna, 1997). Improved and updated version of original code published by P. Blaha, K. Schwarz, P. Sorantin, and S.B. Trickey, Comput. Phys. Commun. **59**, 399 (1990).
[48] K. Schwarz and P. Blaha, Lect. Notes Chem. **67**, 139 (1996).
[49] P. Blaha and K. Schwarz, Int. J. Quantum Chem. **23**, 1535 (1983).
[50] P. Blöchl, O. Jepsen, and O.K. Anderson, Phys. Rev. B **49**, 16 223 (1994).
[51] Y.K. Vohra and A.L. Ruoff, Phys. Rev. B **42**, 8651 (1990).
[52] H. Xia, S.J. Duclos, A.L. Ruoff, and Y.K. Vohra, Phys. Rev. Lett. **64**, 204 (1990).
[53] H. Xia, H. Parthasarathy, Y.K. Luo, Y.K. Vohra, and A.L. Ruoff, Phys. Rev. B **42**, 6736 (1990).
[54] A. Zupan, P. Blaha, K. Schwarz, and J.P. Perdew, Phys. Rev. B **58**, 11 266 (1998).
[55] A. Heiming, W. Petry, J. Trampenau, M. Alba, C. Herzig, H. Schober, and G. Vogl, Phys. Rev. B **43**, 10 948 (1991).